

Analysis of unsteady MHD Williamson nanofluid flow past a stretching sheet with nonlinear mixed convection, thermal radiation and velocity slips

M. Das¹, B. Kumbhakar^{1,*} and J. Singh²

¹Department of Mathematics,
NIT Meghalaya, Shillong-793003, Meghalaya, India

²Department of Mathematics,
JECRC University, Jaipur-303905, Rajasthan, India

Abstract

This article examines the transient MHD convective flow with heat and mass transport of Williamson nanofluid over a stretching sheet in the presence of a chemical reaction. Velocity slips, convective heating and vanishing mass flux conditions at the surface are imposed. As a novelty, the effects of nonlinear thermal radiation, mixed convection, velocity slips and activation energy are incorporated. Such problems find significant applications in aircraft, missiles, gas turbines, etc. Similarity transformations are employed to convert controlling PDEs into a system of ODEs and the resulting nonlinear BVP is solved numerically using *bvp4c*. The effects of various parameters on velocity, temperature and concentration distributions are demonstrated and depicted graphically. However, the numerical values of local skin friction coefficients, Nusselt and Sherwood numbers are tabulated and discussed. The graphs show that the nonlinear convection parameters, for both temperature and concentration, boost the primary flow. Higher values of the velocity slip parameters result in diminishing the flow. The fluid temperature rises as a result of both radiation and convective heating. The activation energy improves the concentration profile within the boundary layer. The current findings would appeal to a broad audience in mechanical engineering, medical sciences, industrial engineering, etc.

Keywords Williamson nanofluid · Thermal radiation · Velocity slip · Convective heating · Activation energy · Chemical reaction

PACS 44.20.+b · 44.25.+f · 44.40.+a · 47.70.Fw · 52.30Cv

Mathematics Subject Classification (2010) 76A05 · 76W05 · 80A20 · 80A32

*Corresponding author. *E-mail address*: bkmath@nitm.ac.in

Nourazar et al. [2] used the HPM to solve an MHD nanofluid flow on a horizontal flat plate with a changing magnetic field and viscous dissipation. A study on the effect of natural convection in viscoelastic fluid past a cone taking viscous dissipation was done by Makanda et al. [3]. In a rotating device, Sheikholeslami et al. [4] examined the nanofluid flow and heat transmission properties between two parallel horizontal plates. Using a fixed wedge with changing wall temperature and concentration, Srinivasacharya et al. [5] investigated the influence of a varied magnetic field on nanofluid flow.

Understanding the boundary layer flow with heat transfer along a stretched sheet has become more significant because of several engineering activities. Extrusion of polymers, paper manufacturing, and other similar processes are examples of chemical engineering and metallurgy applications. The rate of heat transfer between the fluid and stretching surface considering heating and/or cooling has a significant impact on the quality of the final product. As a result, the choice of heating or cooling fluid is critical to the heat transfer rate. In light of the physical relevance of heat transmission across moving surfaces, several researchers have been obliged to publish their discoveries in this area. Crane [6] examined the flow past a stretched plate that is subject to the relation between the velocity and the distance from a slit. This yielded an accurate result. Following Crane's work, MHD viscous flow across a stretched sheet was given by Azimi et al. [7], who discussed the analysis of momentum features in the flow. Dessie and Kishan [8] investigated the effect of viscous dissipation and heat source/sink over a stretching sheet. Mishra et al. [9] studied numerically MHD power-law fluid flow over a stretching sheet taking a non-uniform heat source.

Regarding the MHD heat transfer fluxes, thermal radiation is a crucial factor in controlling heat transfer rate. It may impact many industrial processes such as glass manufacture, gas turbine production, furnace design, and re-entry vehicle engine design. As a result, this generated extensive studies on the influence of heat radiation in hydromagnetic fluxes. Daniel and Daniel [10] explored the impact of thermal radiation and buoyancy force on MHD flow through a stretchable sheet with the help of the homotopy analysis method. Kumbhakar and Rao [11] discussed MHD stagnation point flow of an electrically conducting fluid over a nonlinearly stretching surface considering thermal radiation and viscous dissipation. Kho et al. [12] studied thermal radiation effect in the flow of Williamson nanofluid passing through a stretching sheet. With heat and mass transfer through an unstable stretched surface in a uniform magnetic field, Ishaq et al. [13] explored entropy production and thermal radiation. Alharbi et al. [14] conducted experiments on MHD Eyring-Powell flow in an unstable oscillatory stretching sheet to evaluate the influence of thermal radiation and a heat source/sink. Kumar et al. [15] examined the transient natural/free convective nanofluid flow past a vertical plate with effects of radiation and magnetic field.

According to current trends in chemical reaction analysis, it is essential to create a mathematical model of a system to forecast its performance. Especially in the chemical and hydro-metallurgical sectors, heat and mass transport research during chemical reactions is of great significance. Some examples of

combined heat and mass transfer applications with chemical reaction effects are chemical processing equipment design, fog formation and dispersion, temperature and moisture distribution over agricultural fields and fruit tree groves, crop damage due to freezing, cooling towers, and food processing. An excellent example of a first-order homogeneous chemical reaction is the production of smog. Das [16] examined the effects of thermal radiation and chemical reaction on MHD micropolar fluid flow near an inclined porous plate. Sheikh and Abbas [17] studied chemical reaction impact on MHD viscous fluid flow over an oscillating stretching sheet under the influence of heat generation/absorption. Tarakaramu and Narayan [18] explored the effect of chemical reactions on unsteady MHD nanofluid flow towards a stretchable sheet. Kumar et al. [19] investigated the influence of binary chemical reaction with Arrhenius activation energy on the MHD Carreau fluid flow over a stretched surface. They found that the chemical reaction has a significant impact on the flow. Khan et al. [20] studied the aspects of activation energy and thermal radiation on MHD flow containing Ti_6Al_4V nanoparticle past a stretching sheet. Chu et al. [21] discussed the action of a chemical reaction and activation energy on MHD third grade nanofluid flow past a stretching sheet.

The assumption that the flow field obeys the standard no-slip condition at the sheet is quite common in the preceding research and all relevant references. However, the no-slip criterion is inadequate when the fluid is made up of particle emulsions and polymers. Furthermore, boundary-slipping fluids have crucial technological uses, such as cleaning prosthetic heart valves and interior cavities. In such circumstances, the partial slip is an appropriate boundary condition. Additionally, when micro-scale dimensions are included in the flow field, such a slip is necessary. Slip at the wall boundary significantly alters the fluid's flow behavior and shear stress than no-slip circumstances. Using a low-magnetic Reynolds number assumption, Zheng et al. [22] investigated the slip consequences of Oldroyd-B fluid flow across a plate. Hayat et al. [23] explored velocity slip condition on MHD nanofluid flow past a rotating disk. Amanulla et al. [24] discussed the slip effects on MHD Prandtl flow past an isothermal sphere in a non-Darcy porous medium. Ellahi et al. [25] analyzed the combined impact of slip and entropy generation on MHD flow through a moving plate. Khan et al. [26] explored the significance of slip conditions for a magnetite Jeffrey nanofluid flow over a porous stretching sheet in the existence of thermal radiation and the Soret effect. Das et al. [27] studied multiple slip effects on tangent hyperbolic fluid flow along a stretching sheet considering Soret and Dufour effects, thermal radiation and heat source.

In processes in which high temperatures are involved, convective heat transfer is essential. Consider the following examples: gas turbines, nuclear power plants, thermal energy storage, and so forth. It is more feasible to use convective boundary conditions in industrial and technical processes, such as material drying and transpiration cooling operations [28]. Because of the practical significance of convective boundary conditions in viscous fluids, Many scholars have investigated and presented their findings on this issue. Ramzan et al. [29] investigated the impact of convective heating conditions and Cattaneo-Christov heat

flux with heat production/absorption on MHD 3D Maxwell fluid flow across a bidirectional stretching surface. Nayak et al. [30] studied MHD nanofluid flow over a linearly stretching sheet considering the convective heating boundary constraint along with viscous dissipation, velocity slip, nonlinear thermal radiation and Joule heating. Shah et al. [31] observed simultaneous effects of convective boundary condition and thermal radiation on MHD Carbon nanotubes nanofluid flow across a stretching sheet. Aspects of convective boundary condition, Joule heating, thermal radiation, and a changing heat source/sink were studied in detail by Kumar et al. [32] concerning the flow and heat transfer properties of an electrically conducting Casson fluid due to an exponentially expanding curved surface. Loganathan et al. [33] examined the impact of convective heating, Cattaneo-Christov double diffusion and thermal radiation on MHD Maxwell fluid flow along an extended surface. Recently, Jamshed and Nisar [34] studied convective heating, thermal radiation and heat source effects on Williamson nanofluid flow over a stretching sheet.

Based on the above literature survey, the authors have found that no attempt has been made yet to study the impacts of nonlinear thermal radiation and Arrhenius activation energy on unsteady mixed convective flow of Williamson nanofluid over a stretching surface. Therefore, this research aims to fill such gap by exploring the novel circumstances of nonlinear thermal radiation and activation energy on unsteady MHD convective flow with heat and mass transport of Williamson nanofluid over a stretching sheet in the presence of a chemical reaction. The outcomes of this study may have significant bearings on several practical applications such as in aircraft, missiles, gas turbines, food processing, etc. Numerical solutions are obtained for the velocity, temperature and concentration distributions with the help of *bvp4c* routine of MATLAB software. The impacts of significant flow parameters on velocity, temperature and concentration profiles are illustrated and presented graphically. However, the variations in surface drag-coefficients, Nusselt and Sherwood numbers are discussed using numerical data. Moreover, for a limiting case of the present study, a data comparison is made just to ensure that the obtained results are correct and reliable.

2 Mathematical formulation

Consider a three-dimensional, unsteady and incompressible MHD Williamson nanofluid flow along a stretching surface with velocity slip. Further, the influences of nonlinear thermal radiation and chemical reaction with activation energy are also considered. A physical configuration of the flow problem is demonstrated in Fig. 1. The figure shows that the sheet is positioned in the Cartesian coordinate system (x, y, z) such that the x -axis is along the surface in the direction of flow, y -axis is along the width of the surface, and z -axis is normal to xy plane. A constant magnetic field of magnitude B_0 is applied along the z -direction. The surface is stretched along x and y -directions with velocities $u_w = \frac{ax}{1-\beta t}$ and $v_w = \frac{by}{1-\beta t}$ (a, b being positive constants and β is a parameter

having dimension time^{-1}) respectively. The nanofluid temperature and species concentration at the surface are kept at constant values of T_w and C_w respectively. In contrast, the ambient fluid temperature and species concentration are maintained at constant values of T_∞ and C_∞ , respectively.

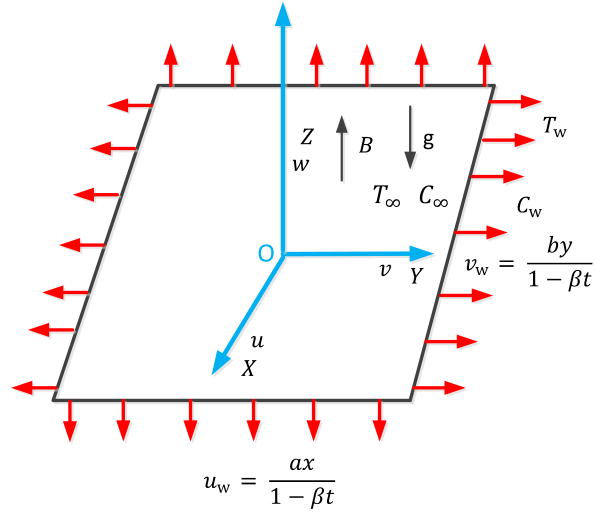


Figure 1: Physical configuration of the problem

Based on the aforementioned assumptions, the governing equations of the current fluid flow (continuity, momentum, energy and species concentration) may be modeled as ([35], [36]):

$$\frac{\partial u}{\partial x} + \frac{\partial v}{\partial y} + \frac{\partial w}{\partial z} = 0, \quad (1)$$

$$\begin{aligned} \frac{\partial u}{\partial t} + u \frac{\partial u}{\partial x} + v \frac{\partial u}{\partial y} + w \frac{\partial u}{\partial z} = & \nu \frac{\partial^2 u}{\partial z^2} + \sqrt{2} \nu \Gamma \frac{\partial u}{\partial z} \frac{\partial^2 u}{\partial z^2} + \frac{\nu \Gamma}{\sqrt{2}} \frac{\partial v}{\partial z} \frac{\partial^2 v}{\partial z^2} - \frac{\sigma B^2(t)}{\rho_f} u \\ & + g [\beta_T (T - T_\infty) + \beta_T^* (T - T_\infty)^2 + \beta_C (C - C_\infty) + \beta_C^* (C - C_\infty)^2], \end{aligned} \quad (2)$$

$$\begin{aligned} \frac{\partial v}{\partial t} + u \frac{\partial v}{\partial x} + v \frac{\partial v}{\partial y} + w \frac{\partial v}{\partial z} = & \nu \frac{\partial^2 v}{\partial z^2} + \sqrt{2} \nu \Gamma \frac{\partial v}{\partial z} \frac{\partial^2 v}{\partial z^2} + \frac{\nu \Gamma}{\sqrt{2}} \frac{\partial u}{\partial z} \frac{\partial^2 u}{\partial z^2} \\ & - \frac{\sigma B^2(t)}{\rho_f} v, \end{aligned} \quad (3)$$

$$\frac{\partial T}{\partial t} + u \frac{\partial T}{\partial x} + v \frac{\partial T}{\partial y} + w \frac{\partial T}{\partial z} = \alpha \frac{\partial^2 T}{\partial z^2} + \tau \left\{ D_B \frac{\partial T}{\partial z} \frac{\partial C}{\partial z} + \frac{D_T}{T_\infty} \left(\frac{\partial T}{\partial z} \right)^2 \right\} - \frac{1}{(\rho c_p)_f} \frac{\partial q_r}{\partial z}, \quad (4)$$

$$\frac{\partial C}{\partial t} + u \frac{\partial C}{\partial x} + v \frac{\partial C}{\partial y} + w \frac{\partial C}{\partial z} = D_B \frac{\partial^2 C}{\partial z^2} + \frac{D_T}{T_\infty} \frac{\partial^2 T}{\partial z^2} - kr(C - C_\infty) \left(\frac{T}{T_\infty} \right)^n e^{-\frac{E_a}{\kappa T}}. \quad (5)$$

The physical boundary conditions for the current problem are given as follows:

$$\left. \begin{aligned} u &= u_w + d_1^* \frac{\partial u}{\partial z}, \quad v = v_w + d_2^* \frac{\partial v}{\partial z}, \quad w = 0, \quad -k \frac{\partial T}{\partial z} = h_f (T_w - T), \\ D_B \frac{\partial C}{\partial z} + \frac{D_T}{T_\infty} \frac{\partial T}{\partial z} &= 0, \quad \text{at } z = 0, \\ u \rightarrow 0, \quad v \rightarrow 0, \quad T \rightarrow T_\infty, \quad C \rightarrow C_\infty &\quad \text{as } z \rightarrow \infty. \end{aligned} \right\} \quad (6)$$

In order to approximate the radiative heat flux q_r , the following Rosseland's approximation for an optically thick fluid is employed (Fatunmbi and Adeniyana [37]):

$$q_r = -\frac{16\sigma^* T^3}{3k^*} \frac{\partial T}{\partial z}. \quad (7)$$

The energy equation has the form after applying expression (7) to equation (4)

$$\frac{\partial T}{\partial t} + u \frac{\partial T}{\partial x} + v \frac{\partial T}{\partial y} + w \frac{\partial T}{\partial z} = \alpha \frac{\partial^2 T}{\partial z^2} + \tau \left\{ D_B \frac{\partial T}{\partial z} \frac{\partial C}{\partial z} + \frac{D_T}{T_\infty} \left(\frac{\partial T}{\partial z} \right)^2 \right\} + \frac{16\sigma^* T^2}{3(\rho c_p)_f k^*} \left\{ T \frac{\partial^2 T}{\partial z^2} + 3 \left(\frac{\partial T}{\partial z} \right)^2 \right\}. \quad (8)$$

The variable aspects of wall temperature, wall concentration and magnetic field are given by the following form [38]

$$T_w(x, t) = \frac{T_0 x u_w}{\nu(1 - \beta t)^{\frac{1}{2}}} + T_\infty, \quad C_w(x, t) = \frac{C_0 x u_w}{\nu(1 - \beta t)^{\frac{1}{2}}} + C_\infty, \quad B(t) = \frac{B_0}{(1 - \beta t)^{\frac{1}{2}}}.$$

To obtain similar solutions of equations (2), (3), (8) and (5) subject to the boundary conditions (6), the following similarity variables are introduced:

$$\left. \begin{aligned} u &= \frac{ax}{1 - \beta t} f'(\eta), \quad v = \frac{ay}{1 - \beta t} g'(\eta), \quad w = -\sqrt{\frac{a\nu}{1 - \beta t}} \{f(\eta) + g(\eta)\}, \\ \theta(\eta) &= \frac{T - T_\infty}{T_w - T_\infty}, \quad \phi(\eta) = \frac{C - C_\infty}{C_w - C_\infty}, \quad \eta = z \sqrt{\frac{a}{\nu(1 - \beta t)}}. \end{aligned} \right\} \quad (9)$$

Substitution of the above similarity variables in equations (2), (3), (8) and (5) yields the following ordinary differential equations:

$$f''' [1 + We_1 f''] + \frac{We_1}{2} L^2 g'' g''' - f'^2 + (f + g) f'' - S \left(f' + \frac{1}{2} \eta f'' \right) - M f' + \lambda (1 + \lambda_1 \theta) \theta + \lambda N (1 + \lambda_2 \phi) \phi = 0, \quad (10)$$

$$g''' [1 + We_2 g''] + \frac{We_2}{2L^2} f'' f''' - g'^2 + (f + g) g'' - S \left(g' + \frac{1}{2} \eta g'' \right) - M g' = 0, \quad (11)$$

$$\theta'' + Pr (f + g) \theta' - Pr \frac{S}{2} (3\theta + \eta \theta') - 2Pr\theta f' + PrNb\theta' \phi' + PrNt\theta'^2 + Rd \{1 + \theta (\theta_w - 1)\}^2 \left[3\theta'^2 (\theta_w - 1) + \{1 + \theta (\theta_w - 1)\} \theta'' \right] = 0, \quad (12)$$

$$\phi'' + PrLe (f + g) \phi' - PrLe \frac{S}{2} (3\phi + \eta \phi') - 2PrLe\phi f' + \frac{Nt}{Nb} \theta'' - PrLe\Gamma_1 \{1 + (\theta_w - 1)\theta\}^n e^{\left(-\frac{E}{1+(\theta_w-1)\theta}\right)} \phi = 0. \quad (13)$$

The dimensionless boundary conditions are stated as

$$\left. \begin{aligned} f'(0) &= 1 + \alpha_1 f''(0), & g'(0) &= \beta_1 + \alpha_2 g''(0), & f(0) &= 0, & g(0) &= 0, \\ \theta'(0) &= -Bi (1 - \theta(0)), & \phi'(0) &= -\frac{Nt}{Nb} \theta'(0), \\ f(\infty) &\rightarrow 0, & g(\infty) &\rightarrow 0, & \theta(\infty) &\rightarrow 0, & \phi(\infty) &\rightarrow 0. \end{aligned} \right\} \quad (14)$$

where

$$\begin{aligned} We_1 &= \sqrt{\frac{2\Gamma^2 a u_w^2}{\nu(1-\beta t)}}, & We_2 &= \sqrt{\frac{2\Gamma^2 a v_w^2}{\beta_1^2 \nu(1-\beta t)}}, & N &= \frac{\beta_C (C_w - C_\infty)}{\beta_T (T_w - T_\infty)}, & S &= \frac{\beta}{a}, \\ \lambda &= \frac{\beta_T g (1 - \beta t) (T_w - T_\infty)}{a u_w}, & M &= \frac{\sigma B_0^2}{a \rho_f}, & L &= \frac{y}{x}, & Pr &= \frac{\nu}{\alpha}, & Le &= \frac{\alpha}{D_B}, \\ Nb &= \frac{\tau D_B (C_w - C_\infty)}{\nu}, & Nt &= \frac{\tau D_T (T_w - T_\infty)}{\nu T_\infty}, & \theta_w &= \frac{T_w}{T_\infty}, & E &= \frac{E_a}{\kappa T_\infty}, \\ \Gamma_1 &= \frac{kr(1-\beta t)}{a}, & \alpha_1 &= d_1^* \sqrt{\frac{a}{\nu(1-\beta t)}}, & \alpha_2 &= d_2^* \sqrt{\frac{a}{\nu(1-\beta t)}}, & \beta_1 &= \frac{b}{a}, \\ Bi &= \frac{h_f}{k} \sqrt{\frac{\nu(1-\beta t)}{a}}, & \lambda_1 &= \frac{\beta_T^* (T_w - T_\infty)}{\beta_T}, & \lambda_2 &= \frac{\beta_C^* (C_w - C_\infty)}{\beta_C}, \\ \delta &= \frac{Q_1(1-\beta t)}{a(\rho c_p)_f}, & Rd &= \frac{16\sigma^* T_\infty^3}{3(\rho c_p)_f \alpha k^*}. \end{aligned}$$

3 Skin-friction coefficients, Nusselt number and Sherwood number

The physical quantities of engineering interest for the present fluid flow problem are the local skin-friction coefficients, Nusselt number and Sherwood number. The skin-friction coefficient measures the shear stress, whereas the Nusselt number and Sherwood number describe the rate of heat and mass transfer at the surface. A low Nusselt number signifies that conductive heat transport is more than the convective heat transfer, whereas a high Nusselt number indicates that convective heat transfer dominates the conductive heat transfer. Thermal engineering devices may be designed more effectively with this in mind. Convective mass transfer is divided by diffusive mass transport, and this ratio is known as the Sherwood number. It is used to conduct mass transfer analyses on systems such as liquid-liquid extraction. Mathematically, the local skin-friction coefficients (C_{fx}, C_{fy}), Nusselt number (Nu_x) and Sherwood number (Sh_x) are expressed as

$$C_{fx} = \frac{\nu}{u_w^2} \left[\frac{\partial u}{\partial z} \left\{ 1 + \frac{\Gamma}{\sqrt{2}} \sqrt{\left(\frac{\partial u}{\partial z}\right)^2 + \left(\frac{\partial v}{\partial z}\right)^2} \right\} \right]_{z=0}, \quad (15)$$

$$C_{fy} = \frac{\nu}{v_w^2} \left[\frac{\partial v}{\partial z} \left\{ 1 + \frac{\Gamma}{\sqrt{2}} \sqrt{\left(\frac{\partial u}{\partial z}\right)^2 + \left(\frac{\partial v}{\partial z}\right)^2} \right\} \right]_{z=0}, \quad (16)$$

$$Nu_x = -\frac{x}{k(T_w - T_\infty)} \left[\left(k + \frac{16\sigma^* T^3}{3k^*} \right) \frac{\partial T}{\partial z} \right]_{z=0}, \quad (17)$$

$$Sh_x = -\frac{x D_B}{D_B (C_w - C_\infty)} \left(\frac{\partial C}{\partial z} \right)_{z=0}. \quad (18)$$

The aforementioned physical values can be expressed in non-dimensional form using the dimensionless variables specified in (9)

$$C_{fx} \sqrt{Re_x} = f''(0) \left[1 + \frac{We_1}{2} \sqrt{f''^2(0) + L^2 g''^2(0)} \right], \quad (19)$$

$$C_{fy} \sqrt{Re_y} = g''(0) \left[1 + \frac{We_2}{2} \sqrt{\frac{1}{L^2} f''^2(0) + g''^2(0)} \right] \sqrt{\beta_1^{-3}}, \quad (20)$$

$$\frac{Nu_x}{\sqrt{Re_x}} = - \left[1 + Rd \{ 1 + (\theta_w - 1) \theta(0) \}^3 \right] \theta'(0), \quad (21)$$

$$\frac{Sh_x}{\sqrt{Re_x}} = -\phi'(0), \quad (22)$$

where $Re_x = \frac{u_w x}{\nu}$ and $Re_y = \frac{v_w y}{\nu}$ are the local Reynolds numbers.

4 Numerical solution

4.1 Methodology

The coupled and highly nonlinear ordinary differential equations (10)-(13) subject to the boundary conditions (14) are solved numerically by employing the *bvp4c* solver in MATLAB. The higher-order equations (10)-(13) are converted into a set of first-order equations. Furthermore, while implementing the numerical technique, the boundary value problem is metamorphosed into an initial value problem by assuming some suitable guess values to those missing initial conditions.

Table 1: Comparison of values of $-f''(0)$ for altered values of M when $\beta_1 = 0.5$

M	$-f''(0)$		
	Present	Oyelakin et al. [39]	Nadeem et al. [40]
0	1.093096	1.09310	1.0932
10	3.342030	3.34204	3.3420
100	10.058166	10.05818	10.058

Table 2: Comparison of values of $-g''(0)$ for altered values of M when $\beta_1 = 0.5$

M	$-g''(0)$		
	Present	Oyelakin et al. [39]	Nadeem et al. [40]
0	0.465206	0.46520	0.4653
10	1.645891	1.64590	1.6459
100	5.020785	5.02080	5.0208

4.2 Validation

The numerical values of $-f''(0)$ and $-g''(0)$ displayed in Tables 1 and 2 have been computed for different values of magnetic parameter M for a specific situation of the current problem, i.e., when $We_1 = We_2 = \lambda = \lambda_1 = \lambda_2 = \alpha_1 = \alpha_2 = N = 0$, $\beta_1 = 0.5$ and $n = 1$ to test the correctness of the obtained results and the reliability of the employed numerical approach. From the tables, it is clearly observed that our results have a firm agreement with the results reported by Oyelakin et al. [39] and Nadeem et al. [40].

5 Results and discussion

This section presents the analysis of the obtained results for the current heat and mass transport phenomenon. The behavior of the flow profiles as well as the physical quantities of practical importance, is investigated in depth with respect to the changes of the emergent parameters. For the computational purpose, we have assumed the parameters' values as $We_1 = We_2 = S = 0.2$,

$N = n = Nt = 0.5$, $Pr = \theta_w = 1.2$, $L = Nb = \lambda = \alpha_1 = \alpha_2 = 0.4$, $Rd = 0.1$, $Le = M = 1.0$, $\beta_1 = 0.7$, $Bi = \lambda_1 = \lambda_2 = K_1 = 0.3$, $E = 0.6$. Throughout the study, the same values for parameters are adopted, while the altered values of the parameters are shown separately in the respective figures.

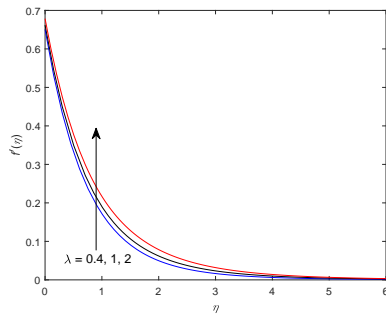


Figure 2: Changes in $f'(\eta)$ vs λ

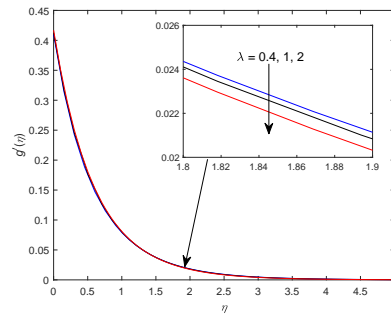


Figure 3: Changes in $g'(\eta)$ vs λ

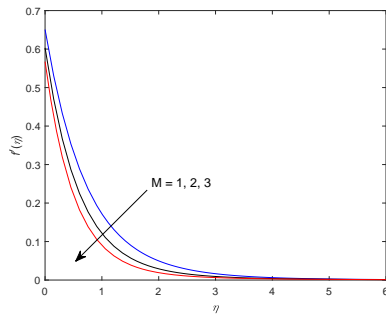


Figure 4: Changes in $f'(\eta)$ vs M

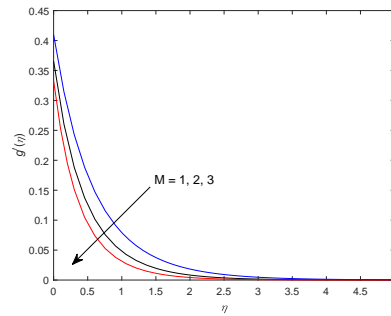


Figure 5: Changes in $g'(\eta)$ vs M

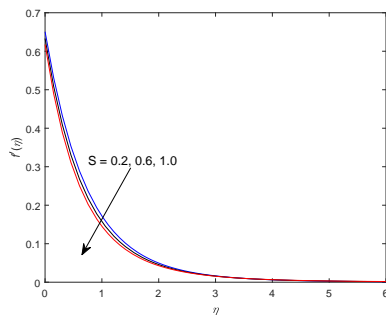


Figure 6: Changes in $f'(\eta)$ vs S

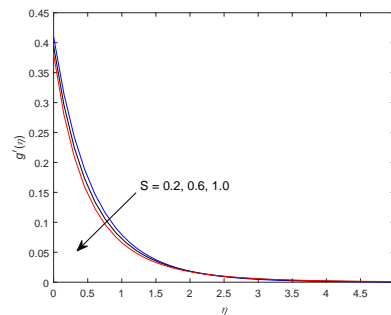


Figure 7: Changes in $g'(\eta)$ vs S

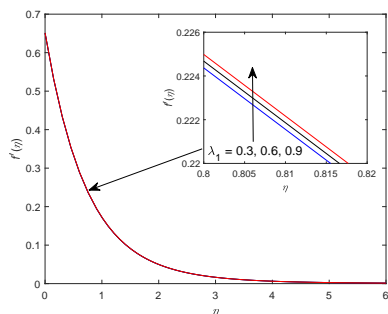


Figure 8: Changes in $f'(\eta)$ vs λ_1

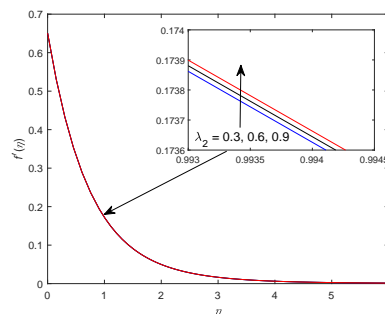


Figure 9: Changes in $f'(\eta)$ vs λ_2

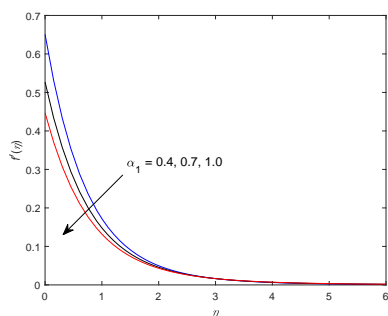


Figure 10: Changes in $f'(\eta)$ vs α_1

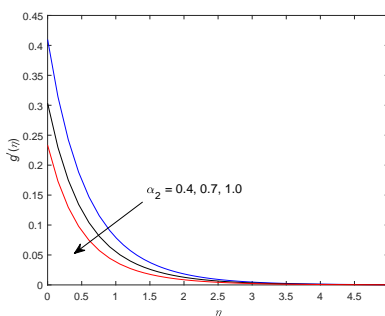


Figure 11: Changes in $g'(\eta)$ vs α_2

Figures 2-11 illustrate the influence of λ , M , S , λ_1 , λ_2 , α_1 and α_2 on the velocity field. Growth in $f'(\eta)$ and reduction in $g'(\eta)$ are observed in Figures 2 and 3. The higher mixed convection parameter contributes to a larger buoyancy force. This powerful force accelerates the primary flow by suppressing the flow in the secondary direction. A significant increase in the magnetic parameter has caused a significant drop in the nanofluid velocity profile. Increased M leads to a corresponding rise in the resistive Lorentz force, which causes the fluid flow to decrease as depicted in Figures 4 and 5. Decreasing nature of $f'(\eta)$ and $g'(\eta)$ for improvement in S is noted in Figures 6 and 7. In Figures 8 and 9, it is noticed that larger values of λ_1 and λ_2 indicate an upsurge in $f'(\eta)$. Temperature and concentration differences arise from nonlinear convection parameters λ_1 and λ_2 that are greater than the equivalent linear convection values. Velocity is therefore emphasized. Figures 10 and 11 express diminishing character of $f'(\eta)$ and $g'(\eta)$ w.r.t. α_1 and α_2 . An increase in velocity slip parameters lead to increase the slip between the fluid and surface of the sheet. So a partial slip velocity moved to the flow field that has the tendency to decelerate the flow.

Figure 12 shows that $\theta(\eta)$ heightens on rising values of M . When the magnetic parameter increases, a stronger Lorentz force is generated. This force

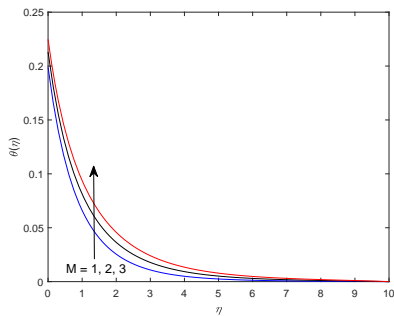


Figure 12: Changes in $\theta(\eta)$ vs M

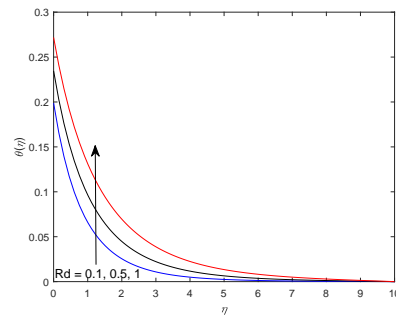


Figure 13: Changes in $\theta(\eta)$ vs Rd

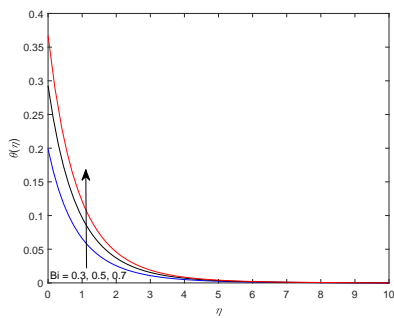


Figure 14: Changes in $\theta(\eta)$ vs Bi

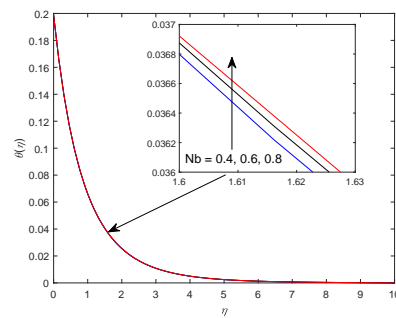


Figure 15: Changes in $\theta(\eta)$ vs Nb

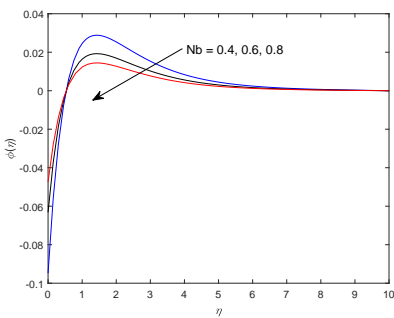


Figure 16: Changes in $\phi(\eta)$ vs Nb

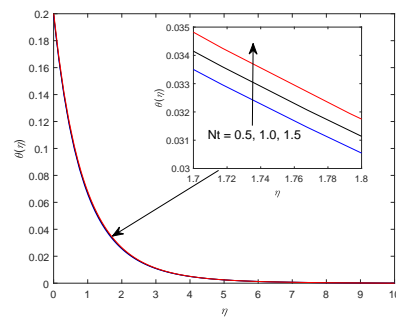


Figure 17: Changes in $\theta(\eta)$ vs Nt

provides resistance against the flow and thereby, the fluid temperature is intensified. Figure 13 elucidates a rising trend for $\theta(\eta)$ on enhanced values of Rd . Improved radiation parameter reduces the mean heat absorption coefficient. As a result, the fluid temperature gets hiked. From Figure 14, an increase in $\theta(\eta)$ is noticed for enlarged values of Bi . An increase in the Biot number leads to

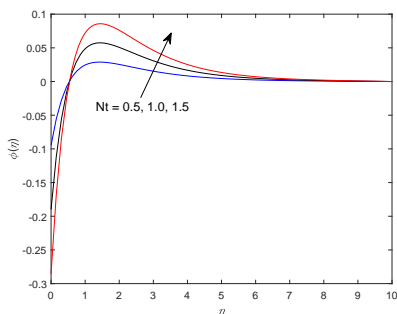


Figure 18: Changes in $\phi(\eta)$ vs Nt

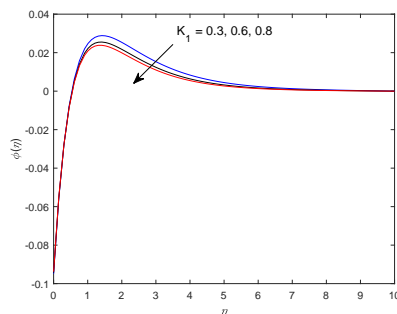


Figure 19: Changes in $\phi(\eta)$ vs K_1

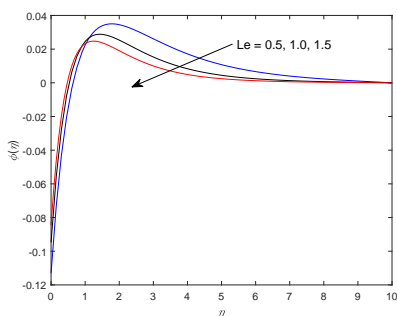


Figure 20: Changes in $\phi(\eta)$ vs Le

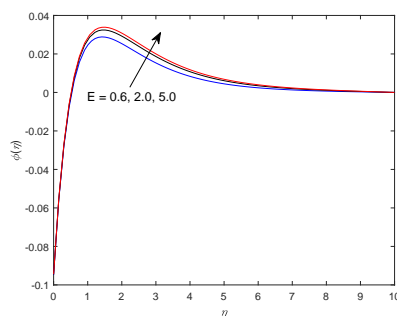


Figure 21: Changes in $\phi(\eta)$ vs E

enhance the heat transfer due to convective heating with hot fluid. So, temperature of the fluid is augmented. Figure 15 shows that when Nb increases, $\theta(\eta)$ decreases near the sheet and takes on an inverse nature far away from it. In reality, a larger Nb causes more Brownian diffusion with lesser viscous forces, and therefore, a hike in the temperature profile is observed. $\phi(\eta)$ is enhanced near the sheet for uplifting Nb values, while a reverse influence is seen away from the sheet, as shown in Figure 16. According to Figure 17, with upsurging values of Nt , $\theta(\eta)$ is increased. Physically, an increase in Nt causes a stronger thermophoretic force, which enriches the fluid's temperature. Figure 18 shows that $\phi(\eta)$ decreases towards the sheet, while the opposite trend is seen further away from the sheet in terms of Nt .

Figure 19 shows that an improvement in K_1 leads to a significant fall in $\phi(\eta)$. A devastating chemical reaction corresponds to a positive K_1 . As a result, an improvement in K_1 causes a decrease in species concentration. In Figure 20, it is seen that for growing values of Le , $\phi(\eta)$ is reduced. Lewis number is basically the relation between thermal diffusivity to mass diffusivity. So, higher Lewis number implies less mass diffusion in the fluid flow. Hence, species concentration is lessened. Figure 21 reveals that there is an upward

Table 3: Numerical values of the skin friction coefficients when $\zeta_C = \zeta_T = 0.4$, $L = \lambda = N = n = 0.5$, $We_1 = We_2 = 1.6$ and $\beta_1 = 0.6$

λ	M	S	λ_1	λ_2	α_1	α_2	$-\sqrt{Re_x}C_{fx}$	$-\sqrt{Re_y}C_{fy}$
0.4	1	0.2	0.3	0.3	0.4	0.4	0.953465	1.833773
	1						0.921040	1.766040
	2						0.871657	1.663539
0.4	2						1.095809	2.137023
	3						1.204741	2.373294
	1	0.6					1.006186	1.945268
		1.0					1.052698	2.044400
		0.2	0.6				0.952571	–
			0.9				0.951679	–
			0.3	0.6			0.953415	–
				0.9			0.953364	–
				0.3	0.7		0.725064	–
					1.0		0.586788	–
					0.4	0.7	–	1.812118
						1.0	–	1.799073

trend in $\phi(\eta)$ with the progress of the parameter E . Boosted E values aid in the speeding up of chemical reactions and hence the species concentration is escalated.

The numerical values of the local skin-friction coefficients for various values of the controlling parameters λ , M , S , λ_1 , λ_2 , α_1 and α_2 are set forth in Table 3. For higher values of M and S , both $\sqrt{Re_x}C_{fx}$ and $\sqrt{Re_y}C_{fy}$ are increased whereas reverse trend is detected w.r.t. λ , λ_1 , λ_2 , α_1 and α_2 . Local Nusselt and Sherwood numbers calculated for flow parameters M , Rd , Bi , Nb , Nt , K_1 , Le and E are described in Table 4. Increasing trend of $\frac{Nu_x}{\sqrt{Re_x}}$ is found for Rd and Bi but opposite nature is noticed for M , Nb and Nt . Growing values of Nt and E imply increasing tendency of $\frac{Sh_x}{\sqrt{Re_x}}$ whereas converse behavior is found w.r.t. Nb , Le and K_1 .

6 Conclusions

The present analysis explores the aspects of nonlinear thermal radiation and activation energy on unsteady convective heat and mass transport phenomena of Williamson nanofluid over a stretching sheet in the existence of Lorentz force and chemical reaction. Moreover, Navier’s velocity slip and convective heating conditions are imposed at the surface boundary. The following are some of the significant outcomes from the simulation of the problem:

- A diminishing nature is observed for the velocity profiles with the improvement in unsteadiness and the intensity of the Lorentz force.

Table 4: Numerical values of the local Nusselt and Sherwood numbers when $Pr = 1.4$, $\theta_w = 1.1$ and $Le = 1.5$

M	Rd	Bi	Nb	Nt	K_1	Le	E	$\frac{Nu_x}{\sqrt{Re_x}}$	$-\frac{Sh_x}{\sqrt{Re_x}}$
1	0.1	0.3	0.4	0.5	0.3	1.0	0.6	0.267377	0.300448
2								0.262851	–
3								0.259108	–
1	0.5							0.361351	–
	1.0							0.474500	–
	0.1	0.5						0.395575	–
		0.7						0.497861	–
		0.3	0.6					0.267364	0.200288
			0.8					0.267357	0.150212
			0.4	1.0				0.267028	0.600074
				1.5				0.266675	0.898864
				0.5	0.6			–	0.300408
					0.8			–	0.300385
					0.3	0.5		–	0.300598
						1.5		–	0.300337
						1.0	2.0	–	0.300487
							5.0	–	0.300502

- The temperature distribution is enhanced as the thermal radiation and the convective heating at the bottom of the surface is boosted.
- The thermophoretic force and the activation energy are found to have strong influence on rising the species concentration far away from the sheet. However, the impact is getting reversed near the sheet.
- The skin friction coefficients are uplifted with the increase of unsteadiness and the magnetic impact.
- There is an enhancement in heat transfer rate at the surface for growing value of Biot number and thermal radiation parameter.
- Rate of mass transfer at the wall is improved as the values of thermophoresis and the activation energy parameters increase.

Acknowledgments

The first two authors are grateful to National Institute of Technology Meghalaya for providing financial assistance and research facilities.

References

- [1] Hayat T, Hussain M, Nadeem S and Mesloub S (2011) Falkner-Skan wedge flow of a power-law fluid with mixed convection and porous medium, *Comput. Fluids*, 49(1):22-28
- [2] Nourazar SS, Matin MH and Simiari M (2011) The HPM applied to MHD nanofluid flow over a horizontal stretching plate, *J. Appl. Math.*, 2011:876437
- [3] Makanda G, Makinde OD and Sibanda P (2013) Natural convection of viscoelastic fluid from a cone embedded in a porous medium with viscous dissipation, *Math. Probl. Eng.*, 2013:934712
- [4] Sheikholeslami M, Abelman S and Ganji DD (2014) Numerical simulation of MHD nanofluid flow and heat transfer considering viscous dissipation, *Int. J. Heat Mass Transf.*, 79:212-222
- [5] Srinivasacharya D, Mendu U and Venumadhav K (2015) MHD boundary layer flow of a nanofluid past a wedge, *Procedia Eng.*, 127:1064-1070
- [6] Crane LJ (1970) Flow past a stretching plate, *J. Appl. Math. Phys.*, 21:645-647
- [7] Azimi M, Ganji DD and Abbassi F (2012) Study on MHD viscous flow over a stretching sheet using DTM-Pade technique, *Mod. Mech. Eng.*, 2(4):126-129
- [8] Dessie H and Kishan N (2014) MHD effects on heat transfer over stretching sheet embedded in porous medium with variable viscosity, viscous dissipation and heat source/sink, *Ain Shams Eng. J.*, 5(3):967-977
- [9] Mishra SR, Baag S, Dash GC and Acharya MR (2020) Numerical approach to MHD flow of power-law fluid on a stretching sheet with non-uniform heat source, *Nonlinear Eng.*, 9(1):81-93
- [10] Daniel YS and Daniel SK (2015) Effects of buoyancy and thermal radiation on MHD flow over a stretching porous sheet using homotopy analysis method, *Alexandria Eng. J.*, 54(3):705-712
- [11] Kumbhakar B and Rao PS (2015) Dissipative Boundary Layer Flow over a Nonlinearly Stretching Sheet in the Presence of Magnetic Field and Thermal Radiation, *Proc. Natl. Acad. Sci., India, Sect. A Phys. Sci.*, 85(1):117-125
- [12] Kho YB, Hussanan A, Mohamed MKA, Sarif NM, Ismail Z and Salleh MZ (2017) Thermal radiation effect on MHD flow and heat transfer analysis of Williamson nanofluid past over a stretching sheet with constant wall temperature, *J. Phys. Conf. Ser.*, 890:012034

- [13] Ishaq M, Ali G, Shah Z, Islam S and Muhammad S (2018) Entropy generation on nanofluid thin film flow of Eyring-Powell fluid with thermal radiation and MHD effect on an unsteady porous stretching sheet, *Entropy*, 20(6):412
- [14] Alharbi SO, Dawar A, Shah Z, Khan W, Idrees M, Islam S and Khan I (2018) Entropy generation in MHD Eyring-Powell fluid flow over an unsteady oscillatory porous stretching surface under the impact of thermal radiation and heat source/sink, *Appl. Sci.*, 8(12):2588
- [15] Kumar MA, Reddy YD, Rao VS and Goud BS (2021) Thermal radiation impact on MHD heat transfer natural convective nanofluid flow over an impulsively started vertical plate, *Case Stud. Therm. Eng.*, 24:100826
- [16] Das K (2012) Influence of thermophoresis and chemical reaction on MHD micropolar fluid flow with variable fluid properties, *Int. J. Heat Mass Transf.*, 55(23-24):7166-7174
- [17] Sheikh M and Abbas Z (2015) Effects of thermophoresis and heat generation/absorption on MHD flow due to an oscillatory stretching sheet with chemically reactive species, *J. Magn. Magn. Mater.*, 396:204-213
- [18] Tarakaramu N and Narayan PVS (2017) Unsteady MHD nanofluid flow over a stretching sheet with chemical reaction, *IOP Conf. Ser.: Mater. Sci. Eng.*, 263:062030
- [19] Kumar RVMSSK, Kumar GV, Raju CSK, Shehzad SA and Varma SVK (2018) Analysis of Arrhenius activation energy in magnetohydrodynamic Carreau fluid flow through improved theory of heat diffusion and binary chemical reaction, *J. Phys. Commun.*, 2:035004
- [20] Khan U, Zaib A, Khan I and Nisar KS (2019) Activation energy on MHD flow of titanium alloy (Ti_6Al_4V) nanoparticle along with a cross flow and streamwise direction with binary chemical reaction and non-linear radiation: Dual Solutions, *J Mater Res Technol.*, <https://doi.org/10.1016/j.jmrt.2019.10.044>
- [21] Chu YM, Khan MI, Khan NB, Kadrye S, Khan SU, Tlili I and Nayak MK (2020) Significance of activation energy, bio-convection and magnetohydrodynamic in flow of third grade fluid (non-Newtonian) towards stretched surface: A Buongiorno model analysis, *Int. Commun. Heat Mass Transf.*, 118:104893
- [22] Zheng L, Liu Y and Zhang X (2012) Slip effects on MHD flow of a generalized Oldroyd-B fluid with fractional derivative, *Nonlinear Anal.: Real World Appl.*, 13(2):513-523
- [23] Hayat T, Muhammad T, Shehzad SA and Alsaedi A (2017) On magnetohydrodynamic flow of nanofluid due to a rotating disk with slip effect: A numerical study, *Comput. Methods Appl. Mech. Eng.*, 315:467-477

- [24] Amanulla CH, Saleem S, Wakif A and AlQarni MM (2019) MHD Prandtl fluid flow past an isothermal permeable sphere with slip effects, *Case Stud. Therm. Eng.*, 14:100447
- [25] Ellahi R, Alamri SZ, Basit A and Majeed A (2018) Effects of MHD and slip on heat transfer boundary layer flow over a moving plate based on specific entropy generation, *J. Taibah Univ. Sci.*, 12(4):476-482
- [26] Khan SA, Nie Y and Ali B (2020) Multiple slip effects on MHD unsteady viscoelastic nanofluid flow over a permeable stretching sheet with radiation using the finite element method, *SN Appl. Sci.*, 2:66
- [27] Das M, Nandi S, Kumbhakar B and Seth GS (2021) Soret and Dufour effects on MHD nonlinear convective flow of tangent hyperbolic nanofluid over a bidirectional stretching sheet with multiple slips, *J. Nanofluids*, 10(2):200-213
- [28] Nandi S and Kumbhakar B (2021) Viscous dissipation and chemical reaction effects on tangent hyperbolic nanofluid flow past a stretching wedge with convective heating and Naviers slip conditions, *Iran. J. Sci. Technol. - Trans. Mech. Eng.*, <https://doi.org/10.1007/s40997-021-00437-1>
- [29] Ramzan M, Bilal M and Chung JD (2017) Influence of homogeneous-heterogeneous reactions on MHD 3D Maxwell fluid flow with Cattaneo-Christov heat flux and convective boundary condition, *J. Mol. Liq.*, 230:415-422
- [30] Nayak MK, Shaw S, Pandey VS and Chamkha AJ (2018) Combined effects of slip and convective boundary condition on MHD 3D stretched flow of nanofluid through porous media inspired by non-linear thermal radiation, *Indian J. Phys.*, 92:1017-1028
- [31] Shah Z, Bonyah E, Islam S and Gul T (2019) Impact of thermal radiation on electrical MHD rotating flow of Carbon nanotubes over a stretching sheet, *AIP Adv.*, 9(4):015115
- [32] Kumar KA, Sugunamma V and Sandeep N (2020) Effect of thermal radiation on MHD Casson fluid flow over an exponentially stretching curved sheet, *J. Therm. Anal. Calorim.*, 140:2377-2385
- [33] Loganathan K, Alessa N, Namgyel N and Karthik TS (2021) MHD flow of thermally radiative Maxwell fluid past a heated stretching sheet with Cattaneo-Christov dual diffusion, *J. Math.*, 2021:5562667
- [34] Jamshed W and Nisar KS (2021) Computational single-phase comparative study of a Williamson nanofluid in a parabolic trough solar collector via the Keller box method, *Int J Energy Res.*, <https://doi.org/10.1002/er.6554>

- [35] Hayat T, Kiyani MZ, Alsaedi A, Khan MI and Ahmad I (2018) Mixed convective three-dimensional flow of Williamson nanofluid subject to chemical reaction, *Int. J. Heat Mass Transf.*, 127(Part A):422-429
- [36] Nandi S, Kumbhakar B, Seth GS and Chamkha AJ (2021) Features of 3D magneto-convective nonlinear radiative Williamson nanofluid flow with activation energy, multiple slips and Hall effect, *Phys. Scr.*, 96:065206
- [37] Fatunmbi EO and Adeniyani A (2020) Nonlinear thermal radiation and entropy generation on steady flow of magneto-micropolar fluid passing a stretchable sheet with variable properties, *Results Eng.*, 6:100142
- [38] Irfan M (2021) Study of Brownian motion and thermophoretic diffusion on non-linear mixed convection flow of Carreau nanofluid subject to variable properties, *Surf. Interfaces*, 23:100926
- [39] Oyelakin IS, Mondal S and Sibanda P (2017) Unsteady MHD three-dimensional Casson nanofluid flow over a porous linear stretching sheet with slip condition, *Front. Heat Mass Transf.*, 8, <https://doi.org/10.5098/hmt.8.37>
- [40] Nadeem S, Haq RU, Akbar NS and Khan ZH (2013) MHD three-dimensional Casson fluid flow past a porous linearly stretching sheet, *Alexandria Eng. J.*, 52:577-582